

Data Driven Modeling for UGI Gasification Process via a Variable Structure Genetic BP Neural Network

Shida Liu, Zhongsheng Hou*, Chenkun Yin

Abstract—An enhanced genetic BP neural network with link switches (EGA-VRBPNN) is proposed in this work to address the data-driven modeling problem for the gasification process inside a UGI gasifier. During gasification processes, the online measured gas temperature is crucial but difficult to model its' dynamics via first principles because of the tremendous complexity of the gasification process, which is mainly reflected from severe changes of the gas temperature versus infrequent and small manipulations of parts of the input variables. EGA-VRBPNN, which incorporates a neural networks with link switches (NN-LS) with an enhanced genetic algorithm (EGA) and the Levenberg-Marquardt (LM) algorithm, can not only learn the relationships between control inputs and system outputs from historical data with the help of optimized network structure through combination of the EGA and NN-LS, but also overcome the drawbacks of gradient-based method and make full use of the network's gradient information to achieve a satisfactory accuracy. A set of data collected from the practical fields are applied to modeling via the EGA-VRBPNN, by which the effectiveness of the EGA-VRBPNN is verified.

Index Terms—Data-driven modeling, UGI gasifier, neural networks with link switches, enhanced genetic algorithm

I. INTRODUCTION

As one of the most viable and practical clean coal technologies for power generation, coal gasification get rapid development in recent years [1]. Until now, there are many kinds of coal gasification technologies and based on the working conditions of these technologies, there exist varies kinds of representative gasifiers being applied in the world, including the UGI gasifier, the Lurgi gasifier, the Texaco gasifier, the Shell gasifier, the Alstom gasifier and the Winkler gasifier, etc.

The UGI gasifier is a kind of atmospheric pressure, fixed bed intermittent device which are applied to syngas production. In China, more than 70% of coal gasification reactors applied in synthetic ammonia manufacturing are UGI gasifiers. Therefore, the optimization and control of the UGI gasifier is highly significant in terms of saving energy.

Inside a UGI gasifier, the temperature of the gasification zone is important but cannot be measured directly. As a substitution, another two indexes, the updraft crude gas temperature (U-Temperature) and the downdraft crude gas

temperature (D-Temperature) are usually considered. If both U-Temperature and D-Temperature keep steady within permissible ranges, the gasification process could be considered to be operated in good conditions. For these reasons, the goal of this paper is to create a mathematical model for the U/D-Temperature inside a UGI gasifier.

In recent years, many first principle modeling methods have been proposed to the gasification process according to different applications and gasifiers, such as methods based on equilibrium models [2, 3], methods based on two-phase models [4, 5], and other modeling methods [6, 7], etc. The implementation of above methods, however, must base on some strict hypothesis which cannot be satisfied in practical industry. Moreover, there are a mass of data generated during the gasification process in the actual industrial production every day, rich enough to contain valuable information about the gasifier. Therefore, creating the mathematical model of gasification process in a data-driven manner is considered.

Many data-driven modeling methods aiming at the gasification field, including fuzzy methods [6, 8], supporting vector machine (SVM) [9], multivariate regression (MVR) [10, 11], etc. Moreover, a special method, the genetic BP neural network (GA-BPNN), which combines the strength of BP neural networks in weight learning and genetic algorithm's capability of parallel searching [12], is widely researched and applied in recent years [13, 14].

Based on the GA-BPNN, an enhanced genetic BP neural network with link switches (EGA-VRBPNN) is proposed in this paper. EGA-VRBPNN can not only learn the input-output dynamics of the gasification process, but also overcome the drawbacks of gradient-based methods and make full use of the network gradient information. Meanwhile, the connection weights and the structure of the network can be adjusted simultaneously during the learning process.

EGA-VRBPNN is implemented in two stages. At the first stage, an initial NN-LS is constructed [15] and an enhance genetic algorithm (EGA), which is proposed based on the properties of the gasification process, is presented. By using EGA, the input-output relationship and the structure of NN-LS describing the gasification process can be optimized simultaneously. During this procedure, EGA is implemented on the basis of following three enhancement techniques. Triple Selection Operation (TSO) is introduced to protect individuals with high fitness and show better performance than the existing 'double selection' [16]; Self-Tuning Crossover Operation (STCO), which is extended from the

Liu S., Hou Z., and Yin C. are with Advanced Control System Laboratory, School of Electronics & Information Engineering, Beijing Jiaotong University, Beijing, China (e-mail: lsdshiwo@hotmail.com; zhshhou@bjtu.edu.cn(* corresponding author); chkyin@bjtu.edu.cn).

This work was supported by the International Cooperation Program (61120106009) of National Science Foundation of China, the Fundamental Research Funds for the Central Universities under Grant (2012JBM008), and the Fundamental Research Funds for the Central Universities (2014YJS024).

classical arithmetic crossover operation but more suitable for the discussed gasification problem; the multi-species strategy is used to partially address the premature convergence problem which may exist during the gasification process. At the second stage, the partially weights connected network obtained at previous stage is further updated by Levenberg-Marquardt (LM) algorithm, by which the network gradient information is fully utilized.

A set of data, which are collected from a practical UGI gasifier in RuiXing Chemical Group, Shandong province, China, is applied to modeling via EGA-VRBPNN, by which the dynamics for the U/D-Temperature is built and the effectiveness of EGA-VRBPNN is verified.

The rest of this paper is as follows. In Section II, the UGI gasification process is briefly introduced and the dynamics of the U/D-Temperature is formulated. In Section III, EGA-VRBPNN for modeling the gasification process is presented. Experimental results are shown in Section IV. A conclusion is drawn in Section V.

II. UGI GASIFICATION PROCESS

A. Principle and Work Flow of UGI Gasification Process

During the gasification process of a UGI gasifier, there exists some complex gas-solid reactions, whose raw materials are coal, steam, oxygen-enriched air and the main output is crude gas, including CO, CO₂, H₂, etc.

The gasification process is briefly described in Fig. 1. As a kind of batch process, the gasification process occurring in a UGI gasifier is intermittent, periodic and repeated. During each gasification cycle (batch) lasting for 150 seconds, all kinds of gas and feedstock are supplied into the gasifier in a fixed sequence for reaction via switching dozens of valves installed on different pipes connected up to the gasifier. Usually, a gasification process consists of several stages as follows.

Firstly, a selected quantity of coal is fed into the gasifier for five seconds and the oxygen-enriched air is blown into the gasifier for 35-40 seconds concurrently. Then the oxidation reactions occur between the oxygen-enriched air and the coal in order to accumulate enough heat that will be used in next

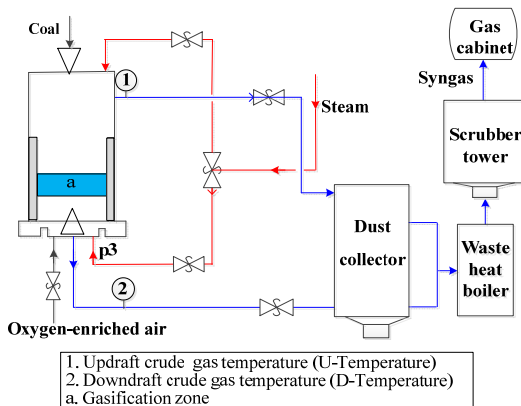


Fig. 1 The briefly layout of gasification process

steps of the gasification cycle. Secondly, the decompressed steam-gas is blown upward to the gasifier for 40-50 seconds such that the burning coal completely reacts with the steam-gas to produce the crude gas. Thirdly, the decompressed steam-gas is blown downward to the gasifier for 50-60 seconds. Comparing with the Stage 2, the difference lies in that the produced crude gas is sent out from pipe with Sensor 2 as Fig. 1 shows.

Then the produced crude gas is sent from the dust collector to filter out the impurities as Fig. 1 shows. After that, the filtered crude gas will enter the heat recovery and desulfurization stage via the waste heat boiler and scrubber tower, respectively. Finally, the syngas is produced and saved into the Gas cabinet.

B. Formulations of U-Temperature and D-Temperature

The gasification zone (marked 'a' in Fig. 1) generating inside the gasifier plays a key role during the gasification process in practice. However, not any direct approach to precisely capture useful information of the gasification zone, especially to measure the temperature, is applicable in the practice until now. To cope with this difficulty, another two indexes about the crude gas are taken into consideration, including the updraft crude gas temperature (U-Temperature) and the downdraft crude gas temperature (D-Temperature), which are measured by Sensor #1 and Sensor #2 in Fig. 1, respectively. If both U-Temperature and D-Temperature keep steady within permissible ranges, the gasification process is considered to be operated in good conditions. Hence, a general MIMO nonlinear dynamic system about U/D-Temperature is considered here.

The first principle modeling methods are applicable on the basis of many strict assumptions. In practical UGI gasification processes, however, most of these assumptions cannot be satisfied. Meanwhile, there are abundant U/D-Temperature data collected from industrial fields every day, reflecting the status and tendency of gasification zone's temperature. Therefore, data driven methods are necessary and possible to develop a dynamic model for the U/D-Temperature for the UGI gasification process.

Many factors, which are stored and monitored by DCS system in the fields, impact on the U/D-Temperature. Some of them are measured online, including the duration of aeration, steam upflow and steam downflow, etc. Because the sum of these three durations is a constant (150 seconds), only the duration of aeration and steam upflow are considered.

Besides, the steam flow, which determines the total quantity of the steam, also can be treated as one factor that influences the U/D-Temperature of one gasifier. Moreover, the thickness of the ash zone, which also affects the gasification zone temperature, can be controlled indirectly by adjusting the speed of the rotating grate whose data can be collected by DCS system. For this reason, the speed of the rotating grate is another important factor affecting the gasification zone's temperature.

According to the abovementioned analysis, a general MIMO nonlinear discrete-time dynamic system as follows is

formulated to describe the dynamic process

$$\mathbf{y}(k+1) = f(\mathbf{u}(k), \mathbf{u}(k-1), \mathbf{y}(k), \mathbf{y}(k-1), \mathbf{w}(k)), \quad (1)$$

where

$$\mathbf{u}(k) = [u_1(k), u_2(k), u_3(k), u_4(k)]^T, \quad (2)$$

$$\mathbf{y}(k) = [y_1(k), y_2(k)]^T, \quad (3)$$

where $y_1(k), y_2(k)$ denote U-Temperature and D-Temperature. $\mathbf{u}(k), \mathbf{y}(k)$ denote control inputs and process outputs, respectively. $f(\cdot)$ is an unknown nonlinear function and k is the sampling index. Specifically, $u_1(k), u_2(k), u_3(k), u_4(k)$ represent the speed of rotating grate, the duration of aeration, the duration of steam upflow, the steam flow, respectively.

Moreover, $\mathbf{w}(k)$ represents noise and some disturbances that have weak impact on the U/D-Temperature, including observable ones as air temperature, air pressure, U-Pressure, D-Pressure. Besides, $\mathbf{w}(k)$ also represent other factors that cannot be measured in a quantitative manner such as the shape of slags inside the rotating grate. Because all data collected from formal working conditions are bounded, the system is considered to be BIBO stable.

III. DATA-DRIVEN MODELING FOR UGI GASIFICATION PROCESS

The MIMO gasification system has some properties which make the modeling process difficult. Firstly, the changes of some inputs are infrequent and small. Averagely, the duration of aeration u_2 and steam upflow u_3 may be not tuned for once in several hours and their values which must be integers often change for one or two within admissible ranges. In such circumstance, it is unable to apply classical frequency identification methods based on least square methods, etc. Secondly, the U-Temperature and D-Temperature are coupled with each other and this coupling cannot be inferred according to the mechanism. It is extremely difficult, if not impossible, to describe the coupling between U-Temperature and D-Temperature using first principles.

The gasification process is formulated as (1)-(3) and the aim of this study is to find a method to obtain the dynamics of (1). For this purpose, an enhanced genetic BP neural network with link switches (EGA-VRBPNN) is proposed. This approach avoids directly analyzing the input-output relationship of the dynamic MIMO model and only the input-output data are used during whole modeling process. EGA-VRBPNN is divided into two stages. At the first stage, a neural network with link switches (NN-LS) is introduced (in section A) and an enhanced genetic algorithm (EGA) is proposed (in section B) to optimize the structure and connection weights of a feedforward neural network described the dynamics of U/D-Temperature. At the second stage, the Levenberg-Marquardt algorithm is proposed to further update the partially weights connected network processed at the first stage.

A. Introduction of Neural Network with Link Switches (NN-LS)

Traditional neural networks usually have a fixed structure.

However, a large network may cause unnecessary implementation cost while a small network cannot achieve a satisfactory accuracy. Here, a MIMO three-layer special neural network is applied, in which the number of links can be tuned.

A neural network with link switches typical network with link switches is shown in Fig. 2, where the switch function is defined as

$$L(l) = \begin{cases} 0, & l \leq 0; \\ 1, & l > 0. \end{cases} \quad (4)$$

The connection weights within NN-LS are

$$w_{ij}^1 = L(l_{ij}) \cdot r_{ij}, \quad (5)$$

$$w_{jk}^2 = L(l_{jk}) \cdot r_{jk}, \quad (6)$$

where $i=1,2,\dots,n_I, j=1,2,\dots,n_h, k=1,2,\dots,n_o$. n_I, n_h and n_o are the number of input nodes, hidden nodes, and output nodes, respectively. Meanwhile, w_{ij}^1 denotes the connection weight between i -th input node and j -th hidden node. w_{jk}^2 denotes the connection weight between j -th hidden node and k -th output node. $L(l_{ij})$ and $L(l_{jk})$ are the link switches indicating the absence or presence of the corresponding link. If the network is fully connected, namely that all the link switches are present, then w_{ij}^1 and w_{jk}^2 will become the classical connection weight r_{ij} and r_{jk} , respectively, as the ones in general NN without link switches. If both n_h and n_o are set 2 in (1), then n_I and n_o becomes 12 and 2, respectively. Thus the input and output of the net at $(k+1)$ -th sample time are

$$\mathbf{I}(k+1) = [u_1(k), \dots, u_4(k), u_1(k-1), \dots, u_4(k-1), y_1(k), y_2(k), y_1(k-1), y_2(k-1)]^T, \quad (7)$$

$$\hat{\mathbf{O}}(k+1) = [\hat{y}_1(k+1), \hat{y}_2(k+1)]^T. \quad (8)$$

Meanwhile, the outputs of hidden layer and output layer are

$$\mathbf{O}_{hidden}(k+1) = \tan\text{-sigmoid}(W^1 \cdot \mathbf{I}(k+1) + \mathbf{b}^1), \quad (9)$$

$$\hat{\mathbf{O}}(k+1) = W^2 \cdot \mathbf{O}_{hidden} + \mathbf{b}^2, \quad (10)$$

where $W^1 = [w_{ij}^1]_{i=1,\dots,12, j=1,\dots,n_h}$ denotes the weight matrix of the links between the hidden layer and the input layer, $W^2 = [w_{jk}^2]_{j=1,\dots,n_h, k=1,2}$ denotes the weight matrix of the links

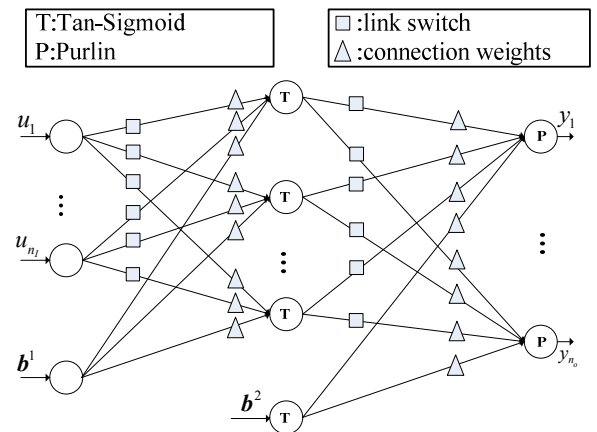


Fig. 2 Structure of neural network with link switches (NN-LS).

between the hidden and output layer; $\mathbf{b}^1 = [b_j^1]_{j=1, \dots, n_h}$ and $\mathbf{b}^2 = [b_k^2]_{k=1, \dots, n_o}$ denote the biases for the hidden nodes and output nodes, respectively. Tan-Sigmoid(\cdot) denotes the tangent sigmoid function

$$\text{Tan-Sigmoid}(x) = (1 - e^{-x}) / (1 + e^{-x}). \quad (11)$$

B. Adjusting NN-LS Structure by Using Enhanced Genetic Algorithm

In most cases, the standard genetic algorithm (SGA) can be used to learn the input-output relationship of a network. In this paper, however, the performance of SGA is influenced by too many optimized variables caused by the all link switches and connection weights of the NN-LS. Moreover, there exists the premature problem caused by properties of gasification process. As a substitution, an enhanced genetic algorithm (EGA) is presented based on SGA to learn the input-output relationship and optimize structure and connection weights of the network. The EGA, in which three enhancement techniques are presented, is implemented as following part 1)-4).

1) Triple selection operation

Before the implementation of EGA, a fitness function, which is utilized to evaluate performance of EGA applied to NN-LS, is firstly defined as

$$\text{fitness} = 1 / \text{MSE}. \quad (12)$$

where

$$\text{MSE} = \sum_{k=1}^{N_{tr}} \frac{[\hat{\mathbf{O}}(k) - \mathbf{O}(k)]^T \cdot [\hat{\mathbf{O}}(k) - \mathbf{O}(k)]}{N_{tr}}, \quad (13)$$

where N_{tr} denotes the size of training set, $\mathbf{O}(k)$ is measured output at k -th sampling time, denoted as

$$\mathbf{O}(k) = [y_1(k), y_2(k)]^T. \quad (14)$$

The objective of EGA is to find an optimal solution (chromosome) to maximize (12).

Each chromosome of a population in EGA is defined as following (15), which consists of all the connection weights and link switches of the constructed NN-LS as shown in Fig. 2.

$$[l_{ij}^1, l_{jk}^2, r_{ij}^1, r_{jk}^2, b_j^1, b_k^2], i = 1, \dots, n_l, j = 1, \dots, n_h, k = 1, \dots, n_o. \quad (15)$$

From (15), the number of genes in a chromosome can be denoted as

$$n_{chr} = 2 \times (n_l \times n_h + n_h \times n_o) + n_h + n_l. \quad (16)$$

It can be seen that n_{chr} is relatively large even if there are a

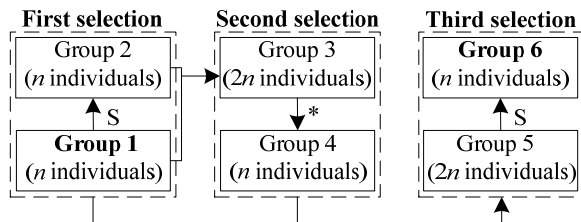


Fig. 3 Schematic diagram of three times selection. S denotes the Roulette selection, * denote three operators, including selection, crossover and mutation.

few hidden nodes within the net. For example, n_{chr} would reach 100 when $n_h > 3$. An individual's fitness might change sensitively with respect to more than 100 genes of the chromosome. In such circumstance, individuals with high fitness values are often easily selected but they also can be accidentally changed by mutation operators at the same time. For these reasons, the first technique called triple selection operation (TSO) is introduced as follows, which can partially address the problems brought by the high dimension of the chromosome.

Fig. 3 illustrates the schematic diagram of TSO. The original population (Group 1, Fig. 3) is composed of n chromosomes. The first selection begins from the Group 1. Then the Group 2 is generated by adopting the classical 'Roulette Selection' with the reproduction probability as

$$\text{prob}_i = f_i / \sum f_i, \quad (17)$$

where f_i is the fitness of the i -th chromosome. Through second selection, crossover, and mutation, the Group 4 is created from Group 3, which combines Group 1 and Group 2. Instead of being considered as the final group, Group 4 is combined with the original Group 1 and then the third selection is applied to the combined group (Group 5). Finally, the Group 6 is created as the children group utilized in next generation.

2) Self-tuning crossover operation and mutation

The selection operation directs the search toward the best existing individuals, however, it does not create any new individuals. Usually, an offspring often has two parents and inherits genes from them. The main operator working on the parents is the crossover operator, which occurred for a selected pair with a crossover rate (P_{cv}). In each new population, there are $p_{cv} \cdot n$ individuals which are needed crossover operations. The second technique proposed here is called self-tuning crossover operation (STCO), which is based on the classical arithmetic crossover operation but more suitable for the research in this paper. In STCO, three candidate offspring are generated and two of them with the largest fitness are selected as the final offspring by completing with each other. By using STCO, the parents information is fully utilized. During this procedure, two offspring can be produced from any two selected parents $\mathbf{P}_a = [g_1^a, g_2^a, \dots, g_{n_{chr}}^a]^T$ and $\mathbf{P}_b = [g_1^b, g_2^b, \dots, g_{n_{chr}}^b]^T$, where superscripts a and b represent the indices of the parents to generate children. After selection operation, STCO is carried out in following three steps.

Step 1: Calculate

$$\mathbf{B}_{\max} = [\max\{g_1^1, \dots, g_1^n\}, \dots, \max\{g_{n_{chr}}^1, \dots, g_{n_{chr}}^n\}]^T, \quad (18)$$

$$\mathbf{B}_{\min} = [\min\{g_1^1, \dots, g_1^n\}, \dots, \min\{g_{n_{chr}}^1, \dots, g_{n_{chr}}^n\}]^T. \quad (19)$$

Here \mathbf{B}_{\max} and \mathbf{B}_{\min} are two artificial chromosomes consisting of genes with maximal value and genes with minimal value, respectively. For the selected parents, calculate

$$\mathbf{P}_{\max} = [\max\{g_1^a, g_1^b\}, \dots, \max\{g_{n_{chr}}^a, g_{n_{chr}}^b\}]^T, \quad (20)$$

$$\mathbf{P}_{\min} = [\min\{g_1^a, g_1^b\}, \dots, \min\{g_{n_{chr}}^a, g_{n_{chr}}^b\}]^T. \quad (21)$$

Step 2: Generate three children as follows

$$C_1 = \alpha_1 \cdot P_a + (1 - \alpha_1) \cdot P_b = [g_1^1, g_2^1, \dots, g_{n_{chr}}^1]^T, \quad (22)$$

$$C_2 = \alpha_2 \cdot P_{\max} + (1 - \alpha_2) \cdot P_{\min} = [g_1^2, g_2^2, \dots, g_{n_{chr}}^2]^T, \quad (23)$$

$$C_3 = \alpha_3 \cdot P_{\min} + (1 - \alpha_3) \cdot P_{\max} = [g_1^3, g_2^3, \dots, g_{n_{chr}}^3]^T, \quad (24)$$

where crossover parameters $\alpha_1, \alpha_2, \alpha_3 \in [0, 1]$ are random numbers in each generation's evolution.

Step 3: Calculate the fitness of C_1, C_2 and C_3 and two of them with largest fitness are selected, denoted as C_a and C_b respectively.

If $f(C_a) > f(P_a), f(C_b) > f(P_b)$, then replace P_a and P_b with C_a and C_b respectively.

If $f(C_a) < f(P_a), f(C_b) < f(P_b)$, then keep P_a and P_b unchanged.

Else, then replace $\max\{f(C_a), f(C_b)\}$ with $\min\{f(P_a), f(P_b)\}$.

During STCO, three children are generated based on three positive random crossover parameters α_1, α_2 and α_3 that are random created in each generation. The introduction of random crossover parameters in SCTO enhances its searching ability since the searching direction can be automatically adjusted so that fast convergence to the optimal solution is guaranteed.

3) Multiple species, migration and real coding

Another technique proposed in EGA focuses on the division of the population into different species [17]. Generally, the premature problem which involves a trade-off between exploration and exploitation often occurs when applying standard GA. To cope with such problem, the multiple species technique is developed here. By using this technique, different search mechanisms in different species are concurrently carried out, and prematurely reaching local minimum is partially avoided. Specifically, three species are adopted in the proposed EGA. Specie 1 and Specie 2 conduct searches individually with increasing focus from a broad but random scope to a local but refined scope. Specie 3 is used to merge the Specie 1 and Specie 2 when EGA is finished. It is worth mentioning that Specie 1 and Specie 2 can be implemented with different evolution mechanisms, including different selection, crossover, mutation operator, as well as different probabilities involved in genetic algorithm, etc. By

doing this, EGA is designed as an independent module for different species.

During the evolution of Specie 1 and Specie 2, the migration operation is adopted in each generation, which involves swapping individuals randomly between two species in each generation. The number of individuals moving between species is controlled by the migration rate (P_{mr}). Generally speaking, a P_{mr} about 5% per generation works well.

Generally, there are many encoding approaches, including binary encoding and real encoding, etc. Some problems involved with a simple on/off mechanism are ideally suitable to apply binary coding. However, if binary encoding is applied to the problems with real numbers just as the one described in this paper, it possibly causes the 'hamming cliff' phenomenon [18]. Hence the real encoding is adopted here.

Remark 1: In fact, EGA-VRBPNN is a kind of pruning algorithms. However, the effect of pruning the links by NN-LS is mainly to reduce the implementation of the network as well as making a small improvement for the modeling accuracy. The parts that greatly increase the algorithm performance are the abovementioned EGA and the L-M algorithm which will be introduced in Subsection C.

4) Adjusting the structure and connection weights of NN-LS by using EGA

In Subsection 1)-3), the EGA has been described and its efficiency compared with SGA can be reflected in Subsection IV-B. In this section, the EGA will be utilized to tune the structure and connection weights of the NN-LS proposed in Subsection III-A.

In EGA, a best chromosome of the contemporary population will be selected in each generation. Meanwhile, all genes in this chromosome are also derived. Specifically, the values of link switches $L(l_{ij}), L(l_{jk})$ can be calculated either 0 or 1 for all i, j, k . Consequently, the existence of w_{ij}^1 and w_{jk}^2 is determined by equation (5) and (6). Hence the structure of NN-LS changes generation by generation until the optimal solution is obtained. As shown in Fig. 4, the initial fully connected feed-forward neural network becomes a partially connected one after learning by EGA. This implies that the cost of implementing the neural network, in terms of processing time, is reduced to some extent.

C. Using Levenberg-Marquardt algorithm to further

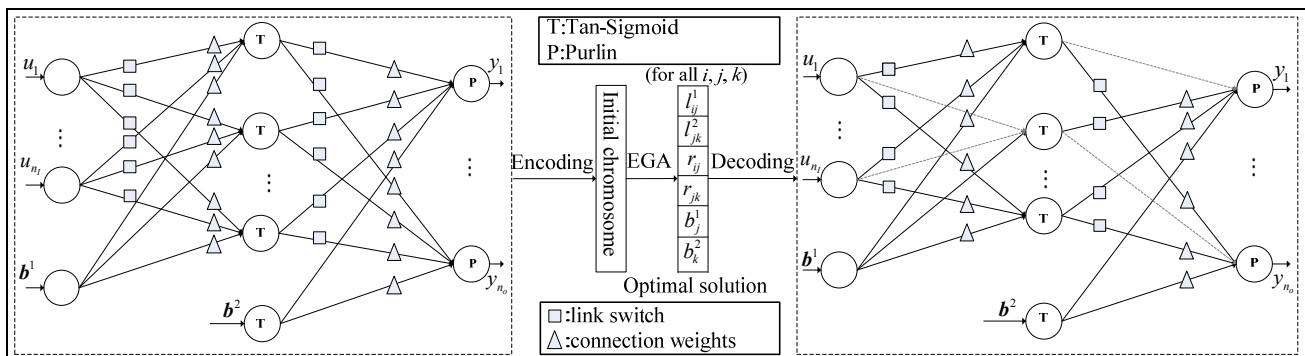


Fig. 4 The process of adjusting the structure and connection weights by using EGA. Some links (dashed line in this figure) will be removed after EGA.

updating connection weights

In Subsection III-B, the structure and connection weights of NN-LS are adjusted simultaneously by incorporating with the proposed EGA. However, a large number of simulation experiments by us prove that although the NN-LS processed by EGA can obtain a higher accuracy than that of SGA, it could not achieve a satisfactory performance for practical application, since the existing characteristics of the UGI gasification process and the noise of data make the population cannot evolve healthily. For these reasons, the (active) connection weights will be further updated to obtain the higher accuracy.

Usually, gradient-based methods exist many drawbacks, especially for the common local minimum problem, such that it is restricted in many neural networks. In this paper, however, this shortcoming is largely overcome by proposed EGA. Therefore, gradient information is possible to be used to deal with the NN-LS processed by EGA. Levenberg-Marquardt algorithm, which is widely applied and has a faster convergent rate and higher accuracy than other common gradient-based algorithms, is considered here. More details about Levenberg-Marquardt algorithm can be found in [19] and the detailed updating process is omitted here.

Remark 2: In some cases, a linear model with less accurate fit may be more sufficient for process control/optimization than a nonlinear one. In this paper, however, the gasification process is so complex that a simple linear model cannot be modelled by a simple linear model.

IV. EXPERIMENTAL RESULTS

To show the usefulness of EGA-VRBPNN, the experiments are carried out using the data collected from the RuiXing Chemical Group, Shandong Province, China. Specifically, the real data applied to the following experiments are collected from 64# gasifier of the factory during April 1-20, 2012.

There exist many variables stored in the database of DCS system. However, only six variables discussed in section II-B are applied to the modeling problem. Specifically, four variables are stored as floats, including U/D-Temperature, Speed of rotating grate and Steam flow. Meanwhile, another two variables are stored as integers, including the duration of aeration and the duration of steam upflow. The original dataset contain 2500 continuous time input-output data pairs. The 1-2000 data pairs are regarded as the training set and the rest 2001-2500 data pairs are the test set.

A. Experimental Results of EGA-VRBPNN

The average absolute error is applied in subsequent analysis to evaluate the accuracy in depth, denoted as

$$\bar{e}_{abs} = \frac{1}{N_{ts}} \left(\sum_{k=1}^{N_{ts}} |\hat{y}(k) - y(k)| \right), \quad (25)$$

where N_{ts} denotes the size of test set, $\hat{y}(k)$ and $y(k)$ denote the network output and the real collected output at k -th sampling time. The parameter setting of EGA-VRBPNN is listed in

TABLE. I, in which P_{cv}^1 , P_{cv}^2 , P_{mu}^1 and P_{mu}^2 are the crossover and mutation probability of Specie 1 and Specie 2, respectively. For comparison, the traditional BPNN are adopted. The BPNN has the same parameters n_i , n_h , n_o , transfer function and training algorithm (L-M algorithm) to EGA-VRBPNN.

1) Results about U-Temperature

The profile of U-Temperature with continuous 500 sampling points in test set by using the BPNN and EGA-NN-LS is shown in Fig. 5. It can be seen that the performance of EGA-VRBPNN is supervisor than that of BPNN, since \bar{e}_{abs} of EGA-VRBPNN is 5.6816°C, improving about 20.6% comparing with BPNN (7.1584°C). Therefore, the accuracy obtained by using EGA-VRBPNN is higher and more acceptable by industrial application than that of BPNN. However, the error of the U-Temperature between the measured value and the network output cannot be further greatly reduced by both methods, since useful information which comes from other adjustable factors influencing the U-Temperature, such as height of the carbon-free layer, type of coal, cannot collected by current DCS system.

2) Results about D-Temperature

The results of D-Temperature with continuous 500 sampling points of test set by using the BPNN and EGA-VRNN are shown in Fig. 6. For D-Temperature, higher accuracy is achieved by applying EGA-VRBPNN, because

TABLE. I
SIMULATION PARAMETERS OF EGA-VRBPNN

Population	200	P_{mu}^1	0.04
Generation	80	P_{mu}^2	0.05
P_{cv}^1	0.6	n_i	12
P_{cv}^2	0.8	n_h	9
N_{tr}	2000	n_o	2
N_{ts}	500	P_{mr}	0.05

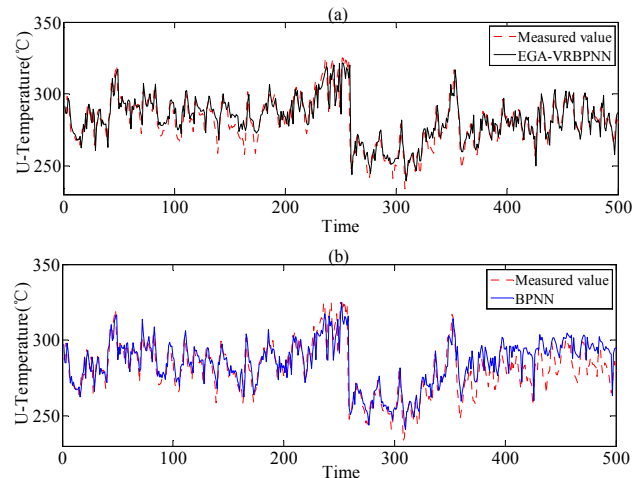


Fig. 5 Results for U-Temperature showing measured values in the test set and the network's output. (a) EGA-VRBPNN with $e_{abs} = 5.6816^\circ\text{C}$. (b) BPNN with $e_{abs} = 7.1584^\circ\text{C}$.

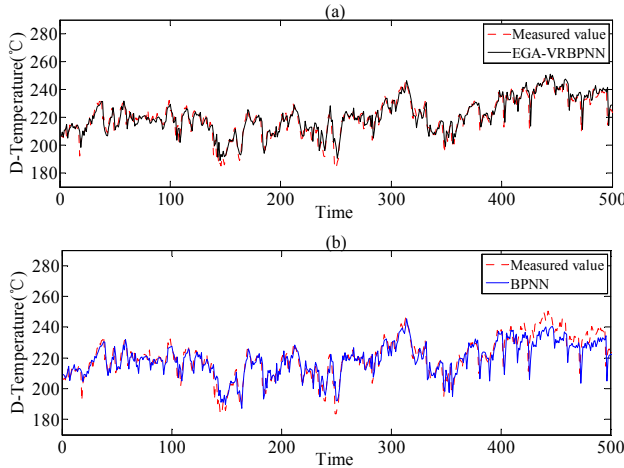


Fig. 6 Results for D-Temperature, showing measured values in the test set and the network's output. (a) EGA-BPNN-LS with $e_{abs} = 3.5505^{\circ}\text{C}$. (b) BPNN with $e_{abs} = 4.4678^{\circ}\text{C}$.

\bar{e}_{abs} of EGA-VRBPNN is about 3.5505°C (Fig. 6(a)), which is 20.5% smaller than that of BPNN (4.4678°C , Fig. 6(b)). Moreover, comparing with Fig. 5, smaller errors are obtained by applying two methods to D-Temperature prediction. The reason is that during the gasification process, the sensor measurement of D-Temperature is closer to the gasification zone so that the smaller interference is affected to D-Temperature than that of U-Temperature.

From Fig. 5 and Fig. 6, it can be summarized that the results obtained by using EGA-VRBPNN has better performance than that of BPNN, since EGA and L-M algorithm play an important role in neural network optimization as stated in Section III. Besides, because of the existing link switches in NN-LS, the structure and connection weights of the network change in each generation during the implementation of EGA. By doing this, higher accuracy with fewer connection links is obtained via EGA-VRBPNN than that of BPNN.

Remark 3: Because that the proposed EGA-VRBPNN is modified based on traditional BPNN, we only make a comparison between EGA-VRBPNN and the BPNN. In fact, being considered from another perspective, the EGA-VRBPNN is also a kind of pruning networks and we also can make a comparison with other existing pruning networks, such as [20]. These studies will be researched in our future works.

B. Results of EGA-VRBPNN Comparing with Other Methods

In order to verify the effectiveness of EGA-VRBPNN, five data driven methods are applied for comparison purpose, including traditional BP neural network (BPNN), standard genetic BP neural network (SGA-NN), enhanced genetic BP neural network (EGA-BPNN), standard genetic neural network with link switches (SGA-VRNN), enhanced genetic neural network with link switches (EGA-VRNN). For the SGA, the population size is 200, the probability of arithmetic crossover, mutation is 0.8 and 0.05, respectively. For BPNN,

TABLE II
IAES OF U/D-TEMPERATURE WITH SIX ALGORITHMS
(ALL RESULTS WERE AVERAGED OVER 30 INDEPENDENT RUNS)

	Algorithms	U-Temperature	D-Temperature
		IAE(°C)	IAE (°C)
1	SGA-VRNN	17367	10109
2	EGA-VRNN	11698	8769
3	BPNN	3783	2351
4	SGA-BPNN	3113	2048
5	EGA-BPNN	2721	1950
6	EGA-VRBPNN	2682	1752

n_h of all abovementioned networks is 9 and the assessment criteria is IAE described as $\sum_{k=1}^{N_g} |\hat{y}(k) - y(k)|$.

TABLE II lists the IAEs of the U/D-Temperature with six algorithms. It can be easily seen that the IAEs of *Algorithm 1-2* are larger than that of *Algorithm 3-6*. It implies that gradient-based method (L-M algorithm here) is necessary for modeling the gasification process. Meanwhile, the IAEs of *Algorithm 4-5* is smaller than that of *Algorithm 3*. These results reflect that the genetic algorithms (including EGA and SGA) play a key role in optimizing the connection weights. Moreover, from IAEs of *Algorithm 4* and *5*, as well as the IAEs of *Algorithm 1* and *2*, it can be seen that no matter whether the BP algorithm is incorporated into the networks or not, EGA has a better performance than that of SGA to optimize the networks. Besides, comparing with *Algorithm 5*, the IAEs of *Algorithm 6* are slightly less than that of *Algorithm 5* while the links of *Algorithm 6* is fewer since the effect of NN-LS. From above analysis, the performance of EGA-VRBPNN is more satisfactory than that of other five algorithms.

V. CONCLUSION

A data-driven modeling algorithm, enhanced genetic BP neural network with link switches (EGA-VRBPNN), is developed to obtain the input-output dynamics of the gas temperature of the UGI gasification process, which is formulated as an unknown nonlinear MIMO dynamic system for the U/D-Temperature of the UGI gasifier. This approach, which is proposed based on the characteristics of UGI gasification, can not only simultaneously learn the input-output relationship and the structure of the network describing the dynamics of proposed U/D-Temperature, but also can overcome the drawbacks of gradient-based methods and make full use of the network gradient information to achieve a satisfactory accuracy. EGA-VRBPNN is successfully applied to a set of data collected from the practical UGI gasifier in a large chemical group and its effectiveness is verified.

In future, we will modelling the gasification process using other algorithms, e.g. the Hopfield neural network and the local modelling algorithm, etc. Furthermore, the data-driven

control problem for the UGI gasification process will also be studied.

[20] N. Fnaiech, F. Fnaiech, B. Jervis, *et al.*, "The combined statistical stepwise and iterative neural network pruning algorithm," *Intelligent Automation & Soft Computing*, vol. 15, pp. 573-589, Mar 2009.

REFERENCES

- [1] D. A. Bell, B. F. Towler, and M. Fan, *Coal Gasification and Its Applications*. Oxford, UK: Elsevier, 2010.
- [2] M. Simone, F. Barontini, C. Nicoletta, *et al.*, "Assessment of syngas composition variability in a pilot-scale downdraft biomass gasifier by an extended equilibrium model," *Bioresource Technology*, vol. 140, pp. 43-52, Apr. 2013.
- [3] T. Srinivas, A. Gupta, and B. Reddy, "Thermodynamic equilibrium model and exergy analysis of a biomass gasifier," *Journal of Energy Resources Technology*, vol. 131, pp. 1-7, 2009.
- [4] E. Gordillo and A. Belghit, "A two phase model of high temperature steam-only gasification of biomass char in bubbling fluidized bed reactors using nuclear heat," *International Journal of Hydrogen Energy*, vol. 36, pp. 374-381, Jan. 2011.
- [5] S. S. Sadaka, A. E. Ghaly, and M. A. Sabbah, "Two phase biomass air-steam gasification model for fluidized bed reactors: part I-model development," *Biomass and Bioenergy*, vol. 22, pp. 439-462, Jun. 2002.
- [6] S. Zanolli, G. Astolfi, and L. Barboni, "Application of a new dataset selection procedure for the prediction of the syngas composition of a gasification plant," in *8th IFAC International Symposium on Advanced Control of Chemical Processes*, Furama Riverfront, Singapore, 2012, pp. 868-873.
- [7] B. Babu and P. N. Sheth, "Modeling and simulation of reduction zone of downdraft biomass gasifier: Effect of char reactivity factor," *Energy Conversion and Management*, vol. 47, pp. 2602-2611, Sep. 2006.
- [8] Z. Shabbir, D. H. Tay, and D. K. Ng, "A hybrid optimisation model for the synthesis of sustainable gasification-based integrated biorefinery," *Chemical Engineering Research and Design*, vol. 90, pp. 1568-1581, Oct. 2012.
- [9] P. Han, D. Li, and Z. Wang, "A study on the biomass gasification process model based on least squares SVM," *Energy Conservation Technology*, vol. 1, pp. 3-7, Jan. 2008.
- [10] P. Kalita, M. Clifford, K. Jiamjiroch, *et al.*, "Characterization and analysis of thermal response of rice husk for gasification applications," *Journal of Renewable and Sustainable Energy*, vol. 5, pp. 013119, Feb. 2013.
- [11] P. Chavan, T. Sharma, B. Mall, *et al.*, "Development of data-driven models for fluidized-bed coal gasification process," *Fuel*, vol. 93, pp. 44-51, Nov. 2012.
- [12] W.-Y. Wang and Y.-H. Li, "Evolutionary learning of BMF fuzzy-neural networks using a reduced-form genetic algorithm," *IEEE Transactions on Systems, Man, and Cybernetics, Part B: Cybernetics*, vol. 33, pp. 966-976, Dec. 2003.
- [13] D. Tong and R. Mintram, "Genetic algorithm-neural network (GANN): a study of neural network activation functions and depth of genetic algorithm search applied to feature selection," *International Journal of Machine Learning and Cybernetics*, vol. 1, pp. 75-87, Sep. 2010.
- [14] P. P. Palmes, T. Hayasaka, and S. Usui, "Mutation-based genetic neural network," *IEEE Transactions on Neural Networks*, vol. 16, pp. 587-600, May. 2005.
- [15] F. H. Leung, H. Lam, S. Ling, *et al.*, "Tuning of the structure and parameters of a neural network using an improved genetic algorithm," *IEEE Transactions on Neural Networks*, vol. 14, pp. 79-88, Jan. 2003.
- [16] D. Guyer and X. Yang, "Use of genetic artificial neural networks and spectral imaging for defect detection on cherries," *Computers and Electronics in Agriculture*, vol. 29, pp. 179-194, Dec. 2000.
- [17] M. Perry, C. Koh, and Y. Choo, "Modified genetic algorithm strategy for structural identification," *Computers & Structures*, vol. 84, pp. 529-540, Nov. 2006.
- [18] I. G. Damousis, A. G. Bakirtzis, and P. S. Dokopoulos, "Network-constrained economic dispatch using real-coded genetic algorithm," *IEEE Transactions on Power Systems*, vol. 18, pp. 198-205, Feb. 2003.
- [19] B. M. Wilamowski and H. Yu, "Improved computation for Levenberg-Marquardt training," *IEEE Transactions on Neural Networks*, vol. 21, pp. 930-937, Jun. 2010.